

## Exploring filament galaxies using *AstroSat*/ UVIT

DIVYA PANDEY,<sup>1,2</sup> KANAK SAHA,<sup>3</sup> AND ANANTA C. PRADHAN<sup>2</sup>

<sup>1</sup>*Aryabhata Research Institute of Observational Sciences, Manora Peak, Nainital 263 002, India*

<sup>2</sup>*Department of Physics and Astronomy, National Institute of Technology, Rourkela, Odisha 769 008, India*

<sup>3</sup>*Inter-University Centre for Astronomy & Astrophysics, Postbag 4, Ganeshkhind, Pune 411 007, India*

### ABSTRACT

We present results from our deep Far-ultraviolet (FUV) survey using *AstroSat*/UVIT of a filamentary structure at  $z \sim 0.072$ . A total of four filaments comprising 58 galaxies were probed in our study. We detect 18 filament galaxies in our FUV observation. All filament galaxies are further classified based on their photometric color, nuclear activity, and morphology. The filaments contain galaxies with mixed stellar population types and structures. We do not detect galaxies in our UVIT survey up to a distance of 0.4 Mpc from the filament axis, implying a dearth of recent star formation in the inner region of filaments. We witness an increase in FUV specific star formation rate (sSFR) of filament galaxies with increasing distance from the filament spine ( $D_{\text{fil}}$ ). On the contrary, no such gradient in FUV sSFR with cluster-centric distance is observed in the case of cluster galaxies. The high stellar mass filament galaxies ( $M_{\star} \sim 10^{11} M_{\odot}$ ) were more star-forming than cluster galaxies in a fixed mass range. The FUV morphology of some filament galaxies detected in the filament outskirts ( $D_{\text{fil}} \sim 0.9$  Mpc) is comparable to or slightly extended than their optical counterpart. The mass assembly of galaxies probed by estimating ( $FUV - r$ ) color gradients show that more centrally star-forming galaxies reside closer to the filament axis regardless of stellar mass. Our results prove that the likelihood of merger interaction and gas starvation increases on approaching the filament spine. We report a definitive and in-homogeneous impact of filaments on the galaxies residing inside them.

*Keywords:* Large-scale structure of the universe(902) — Ultraviolet astronomy(1736) — Galaxy evolution(594) — Galaxy environments(2029) — Star formation(1569)

### 1. INTRODUCTION

Filaments are the most visually dominant component of the cosmic web. Around 50% of galaxies or baryonic mass in the Universe resides within filaments while the structure occupies only  $\sim 5\%$  of the cosmic volume (Cautun et al. 2014). Filaments inhabit the spaces between massive clusters and inside voids (Tempel et al. 2014). Filaments are not just an assembly of galaxies; they provide a dynamical pathway in channeling the galaxies to massive clusters. Apart from the cool baryonic matter in galaxies, filaments are shown to be the carrier of warm-hot intergalactic matter (WHIM; Galárraga-Espinosa et al. 2021). The filamentary pattern in the cosmic web is well-illustrated both in simulations (Col-

berg et al. 2005; Cautun et al. 2014) as well as observations (e.g., Durret et al. 2003; Porter & Raychaudhury 2005). The detection of filaments within the cosmic web is an intricate task due to their low environmental density. There are various algorithms available for extracting filaments in the cosmic web, such as Bisous (Tempel et al. 2014), DisPerSE (Sousbie et al. 2011), NEXUS+ (Cautun et al. 2013, 2014), etc.

Several large-scale phenomena, such as cosmic web enhancement and detachment, are reported to occur inside filaments. A few filament galaxies are shown to host ionized gas clouds in their circumgalactic region due to cosmic web enhancement (Vulcani et al. 2019). On the other hand, it is theoretically indicated that galaxies experience gas starvation caused by cosmic web detachment inside filaments due to the non-linear interaction of the cosmic web (Aragon Calvo et al. 2019). These physical mechanisms affect the ongoing star formation activity of the constituent galaxies. Filaments also affect

their resident galaxies dynamically due to non-uniform large-scale matter distribution (Lee & Pen 2000; Tempel & Libeskind 2013). Therefore, it is evident that the filaments significantly impact the evolution of the galaxies inside them.

There are a number of observation- (e.g., Kuutma et al. 2017; Mahajan et al. 2018; Lee et al. 2021) and simulation-based (e.g., Singh et al. 2020) studies performed to probe the structural and physical properties of filament galaxies. Most of these analyses are based on optical imaging and spectroscopic datasets. The local environment density around filament galaxies and the distance of galaxies from the filament spine are found to impact their growth (Bonjean et al. 2020). Studies focusing on undermining the properties of galaxies as a function of their distances from the spine of filaments found that the passive galaxy fraction increases closer to the filament axis (Kuutma et al. 2017; Laigle et al. 2018; Singh et al. 2020; Bonjean et al. 2020). The authors report a morphological transformation of filament galaxies from late- to early-type, followed by a suppression in ongoing star formation when approaching the filament spine from the void environment. An increased likelihood of finding bright and red galaxies at a similar large-scale luminosity density is observed in filaments than outside them due to a higher number of elliptical galaxy populations (Poudel et al. 2017). Although filaments are found to host red and passively evolving galaxies, they are comparatively less massive and bluer than their counterpart in the clusters (Mahajan et al. 2018). Meanwhile, filaments are reported to act as a stimulator for star formation activities in galaxies, e.g., Darvish et al. (2014) uncovers the possibility of enhanced gas accretion in filament galaxies through inter-filamentary channels. Filaments provide an active environment to trap cold gas, assist its cooling, and enhance star formation activity (Liao & Gao 2019). The discussion above reveals an inhomogeneity in the star formation properties among filament galaxies.

The ultraviolet (UV) emission broadly divided into two wavelength ranges, far-UV (FUV) and near-UV (NUV), from galaxies is an ideal tracer of recent star formation in galaxies (Gil de Paz et al. 2007). A few investigations in the past have probed the properties of filament galaxies with the help of UV and UV-optical colors (e.g., Mahajan et al. 2018; Lee et al. 2021) using observations from Galaxy Evolution Explorer (*GALEX*, Morrissey et al. 2007). The authors examine the gradient in UV colors of filament galaxies when approaching the filament spine. Another study inspected the changes in *GALEX*-based NUV star formation rates (SFRs) and stellar mass of spiral galaxies along filaments (Alpaslan

et al. 2016). These analyses hinted towards a definitive transformation in UV properties along the filament. However, none of the studies have focused on deep FUV properties of filament galaxies as *GALEX* All-sky Imaging (AIS) survey, which covers a maximum portion of the sky and has a typical exposure time of 100 s with a resolution of 5'' (Morrissey et al. 2007). The FUV emission provides a clear separation between recently star-forming and passive galaxies. The average timescale of FUV emission is roughly 0.1 Gyr, even shorter than the NUV emission timescale of about 1 Gyr (Gil de Paz et al. 2007). Therefore, deep and spatially-resolved FUV observation of filaments could help us trace the ongoing recent star formation along the filaments.

This work is based on a proposed deep FUV survey of filamentary structure conducted by *AstroSat*/ Ultraviolet Imaging Telescope (UVIT, Tandon et al. 2017). The rectangular box shown in Figure 1 encloses the targeted filamentary structure. An enhanced spatial resolution ( $\approx$  three times better than *GALEX*) and greater sensitivity of UVIT would help us identify recently star-forming galaxies in the filaments, which may be undetected in previously done shallow UV imaging surveys. We have conducted a similar deep UVIT survey of the Bootes void (red circle in Figure 1; Kirshner et al. 1981). The observations led to the detection of a few void galaxy candidates, which were undetected in *GALEX* observation. We reported a distinct blueward shift in color of void galaxies compared to a sample of nearby galaxy (Pandey et al. 2021). Voids and clusters are the rarest and densest environments, respectively. At the same time, filaments are thought to represent the intermediate environment density. A detailed understanding of star formation activity across environments will be possible when enough studies explore these environments in FUV. Our FUV observation of the filaments would be utilized to investigate the gradient in UV emission across its width. We plan to compare the results with galaxies in different environments.

Physical phenomena such as galaxy mergers, gas starvation and accretion, etc., occur inside filaments. These mechanisms, along with the star formation history of a galaxy, can lead to different stellar mass assembly mechanisms (Lin et al. 2019). We would compare the FUV morphology of filament galaxies with their optical to identify mergers or gas accretion signatures. Moreover, we plan to utilize multi-wavelength observations to probe the mass assembly of filament galaxies to highlight the dominant physical mechanisms responsible for galaxy evolution in filaments. This study would provide insights into the role of cosmic filaments in shaping the star formation activity of galaxy populations.

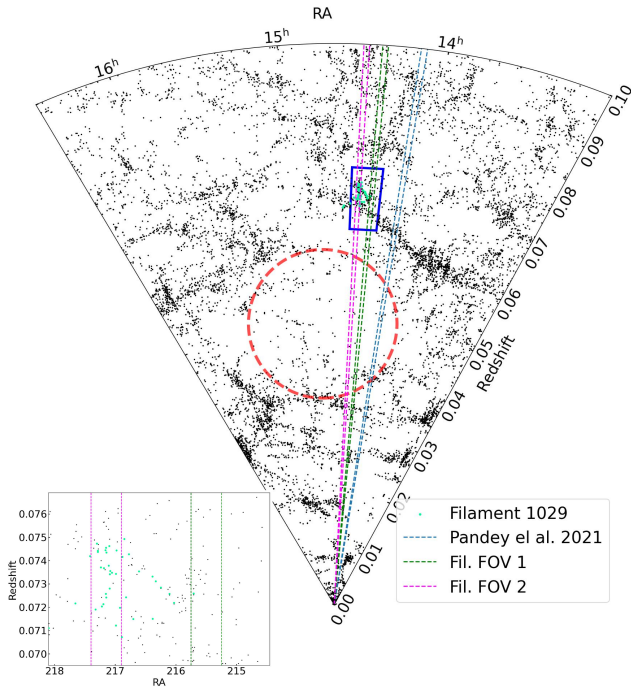


**Figure 1.** Redshift cone diagram of galaxies in the line-of-sight of UVIT observation. Each black dot in the figure represents a galaxy taken from *SDSS* DR 16. Blue rectangular box surrounds the filamentary structure observed in our UVIT survey. The box is zoomed in the inset plot. The galaxy distribution in light-green color highlights one of the filaments (Filament ID 1029 in [Tempel et al. \(2014\)](#)) studied in this work. The set of magenta and green lines encloses the UVIT FOVs observed in the present study. The red circle represents the boundary of the Bootes void while the pair of blue line encloses the FOV observed by us to examine the properties of void galaxies ([Pandey et al. 2021](#)).

This paper is organized as follows: Section 2 describes the observational data used in the work and UVIT data reduction techniques followed, and Section 3 explains our methodology applied in extracting filament galaxies from UVIT observations. We derive the photometric and chemical properties of filament galaxies in Section 4. Various aspects of FUV emission of the sample, such as morphology and FUV SFRs are discussed in Section 5. In Section 6, we examine the mass assembly of filament galaxies. Our findings are discussed in Section 7. A standard  $\Lambda$ CDM cosmology with  $\Omega_M = 0.3$ ,  $\Omega_\Lambda = 0.7$ , and  $H_0 = 70 \text{ km s}^{-1} \text{ Mpc}^{-1}$  is assumed in this paper.

## 2. DATA

### 2.1. Observations

We primarily use proposed *AstroSat*/UVIT data observed in BaF2 filter centered at  $\lambda_e = 1541$

Å (Observation ID: A09\_127T01\_9000003816, A09\_127T03\_9000003820; PI: Divya Pandey). The total field-of-view (FOV) of the UVIT channel is  $28'$  in diameter. The pixel scale of the reduced image =  $0.417''$ , whereas the zero-point of the filter is  $\sim 17.78 \text{ mag}$  ([Tandon et al. 2020](#)). Under the proposal, we observe a filamentary structure at  $z \sim 0.073$ . The observed structure is located close to one of the largest voids in the northern hemisphere, the Bootes void (See Figure 1). We proposed to observe the structure in two FOVs with an exposure time of 7 kilo seconds each. The central coordinates of the two pointing are:  $\alpha = 217.15^\circ$ ,  $\delta = 46.12^\circ$  (FOV2) and  $\alpha = 215.85^\circ$ ,  $\delta = 46.1^\circ$  (FOV1). Figure 1 shows the direction of UVIT pointings on the cosmic web.

Apart from the UV survey, we use archival imaging and spectroscopic data from Sloan Digital Sky Survey Data Release 16 (*SDSS* DR 16, [Ahumada et al. 2020](#)) and Galaxy Evolution Explorer (*GALEX*, [Morrissey et al. 2007](#)) in this work.

### 2.2. UVIT data reduction and analysis

We obtain the raw Level 1 version of the observations from *AstroSat* data archive<sup>1</sup>. The level 1 data is fed into CCDLAB ([Postma & Leahy 2021](#)). CCDLAB is an automated pipeline used for reducing the L1 version of UVIT data into science-ready images. The data reduction includes drift correction, flat-field correction and is further corrected for additional distortion and fixed noise pattern. The corrected images from different orbits are stacked together through the centroid alignment process to obtain a deep, science-ready image. CCDLAB removes frames containing large numbers of photon counts due to cosmic ray shower, leading to a reduction in the total exposure time of the image. The effective exposure time ( $t_{\text{exp}}$ ) of the final images was 5.7 ks and 6.3 ks. The world coordinate system (WCS) was assigned to the final images using *Astroquery* ([Ginsburg et al. 2019](#)) appended with CCDLAB. *Astroquery* uses the GAIA ([Gaia Collaboration et al. 2016](#)) catalog to assign coordinates to each pixel in the final image. The mean error in the astrometry was  $\approx 0.''28$ . Along with the science-ready images, we get corresponding exposure maps as an output from the CCDLAB.

We run source extractor ([Bertin & Arnouts 1996](#)) for detecting sources observed in the two sets of FUV images. The background is detected in automated mode. The detection and analysis threshold is fixed at  $1.5\sigma$  for source extraction and photometry. We consider the

<sup>1</sup> [https://webapps.issdc.gov.in/astro\\_archive/archive/Home.jsp](https://webapps.issdc.gov.in/astro_archive/archive/Home.jsp)

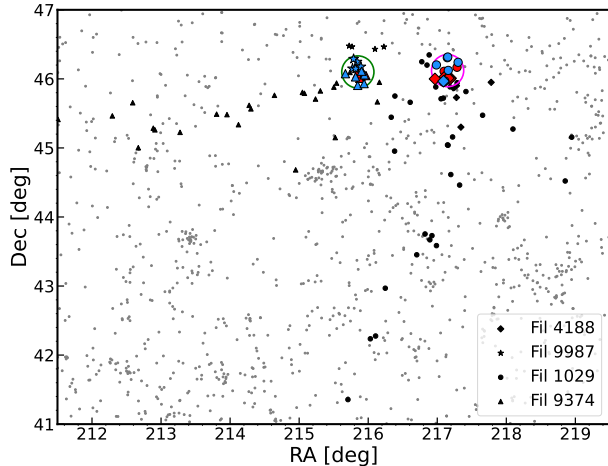


**Figure 2.** Sky map showing the distribution of galaxies in the line of sight of our observation. Different symbols for each filament are used to indicate the number of galaxies present in each of the four filaments. Green and magenta circles enclose the UVIT FOV. The galaxies depicted by blue markers were detected in the FUV survey whereas the red colored markers within FOVs represent filament galaxies which were undetected.

minimum number of pixels required to classify an intensity distribution as a source (DETECT\_MINAREA) to be 9. The  $3\sigma$  limiting magnitudes for our observation in FOV 1 and FOV 2 are 24.79 mag and 25.07 mag, respectively. We detected a total of 3574 sources combining both the FOVs. We perform Petrosian photometry to measure the integrated magnitude of the detected sources. We expect to detect irregular and disk galaxies in our UVIT FOVs wherein the Petrosian apertures may recover nearly all flux from an exponential light distribution (Blanton et al. 2001).

### 3. IDENTIFYING FILAMENT GALAXIES

Only a fraction of the detected sources in our the FUV observation belong to the filaments. Hence, the identification of filament galaxies is imperative part of our study. Multiple catalogs employ various algorithms to find filaments and associated galaxies in large-scale structures (Tempel et al. 2014; Carrón Duque et al. 2022; Alpaslan et al. 2014). We use a catalog given by Tempel et al. (2014, hereafter Tempel catalog) in our study. The authors use the Bios model to detect filaments in an extensive database of galaxies observed with *SDSS*. The catalog provides a detailed list of filaments and constituent filament galaxies. The information regarding the distance from the nearest filament spine ( $D_{\text{fil}}$ ), co-moving distance, integrated magnitudes, and optical luminosities for each filament galaxy are included in the catalog.

**Table 1.** Details of the filament observed in our UVIT observation.

Fil. ID	Length	Total Galaxies	FUV <sub>UVIT</sub>	FUV <sub>GALEX</sub>
(1)	(2)	(3)	(4)	(5)
9987	3 Mpc	7	5	5
9374	7.55 Mpc	19	6	5
1029	13.69 Mpc	24	6	2
4188	3 Mpc	9	1	0

Col (1): Filament identity from Tempel et al. (2014), Col (2): Length of each filament, Col (3): Total number of galaxies present in each filament within 1 Mpc from the filament spine, Col (4): Number of galaxies detected in UVIT FUV and Col (5): Number of galaxies present in GALEX FUV catalog .

We matched our UVIT source catalog with the Tempel catalog within a radius of  $\sim 2.''5$  to identify filament galaxies in our FUV observations. The detected galaxies belong to four different filaments (Filament ID: 1029, 4188, 9987, and 9374 in the Tempel catalog) of different lengths. The four filaments together contain 58 galaxies, of which 18 were detected in the UVIT sample. We restrict our filament sample up to  $D_{\text{fil}} = 1$  Mpc, as previous reports on filament galaxies point out that the filament considerably impacts the properties of galaxies situated within 1 Mpc distance from their axis (Tempel & Tamm 2015; Tempel et al. 2015). A sky map depicting the distribution of galaxies in each filament is shown in Figure 2. The inset figure highlights the UVIT FOVs, UVIT targeted and detected galaxies. The red-colored markers within FOVs represent filament galaxies undetected in our survey, whereas the galaxies depicted by blue markers were detected in the FUV survey. Prior to UVIT, a shallow FUV survey ( $t_{\text{exp}} \sim 100$  s) of the observed FOVs was conducted by *GALEX*. We find that six of the 18 filament galaxies detected by UVIT remained missing in *GALEX* AIS catalog. In other words, these filament galaxies are newly detected in our UVIT survey. Table 1 consists of information on each filament, their constituent galaxies, and a comparison between filament galaxies detected by UVIT and *GALEX* AIS observation.

We extract Petrosian magnitudes corresponding to all *SDSS* broadband filters and spectroscopic information for all 58 galaxies from *SDSS* DR 16. The magnitudes used in this work are corrected for Galactic extinction using Galactic dust extinction maps provided by Schlegel et al. (1998).

### 4. PROPERTIES OF FILAMENT GALAXIES

We study the star-forming, nuclear, and structural properties of all 58 galaxies in the four filaments. As shown in Figure 2, only a portion of these filaments were observed with UVIT. Therefore, we create two subsets among the total galaxies observed with UVIT (within 1 Mpc from the nearest filament axis): the FUV detected and FUV undetected galaxies. The histogram shown in the upper left panel of Figure 3 highlights the cross-section distribution of galaxies inside filaments from the filament axis for the entire sample and both subsets. The filaments seem to be more dense in the inner region. Interestingly, we detect no galaxy in our FUV observation up to  $D_{\text{fil}} \approx 0.4$  Mpc.

#### 4.1. Color-magnitude diagram

We use optical  $g-r$  vs.  $M_r$  color-magnitude diagram (CMD) to classify all 58 filament galaxies into the blue cloud, red sequence, and green valley galaxies (Blanton et al. 2005; Salim 2014). The blue cloud contains star-forming galaxies, mostly disk-dominated spirals, and irregulars. The red sequence comprises star formation quenched galaxies. Lenticular and elliptical galaxies mostly dominate this region. The intermediate region between the two modes of distribution is known as the green valley, where galaxies with intermediate star formation histories lie. The parallel lines dividing the CMD are given by Blanton et al. (2005). The background galaxies in the sample are taken from *SDSS* DR 16 within  $z < 0.1$ .

As seen in the upper right panel of Figure 3, our filament sample is spread across the blue cloud and green valley region. We detect a comparable population of star-forming galaxies and green valley galaxies in our FUV survey. On the contrary, we only detected star-forming and blue galaxies in our previous study of the Bootes void (Pandey et al. 2021). We highlight the dominance of green valley galaxies in filaments which contain a mix of stellar population. Such galaxies are in transition phase where the star formation is declining but not entirely ceased. Galaxy interactions and mergers, feedback from active-galactic nuclei (AGN) are few physical mechanisms that can drive a galaxy to this state (Salim 2014). The galaxies present in filaments studied by us are brighter than  $M_r \sim -20$  mag. However, previous reports have confirmed the presence of faint dwarf galaxies in filament environment as well (Lee et al. 2021).

#### 4.2. BPT diagram

The BPT (Baldwin, Phillips, and Terlevich, Baldwin et al. 1981) diagram is ubiquitously used to classify and understand the ionization sources of galaxies based on their emission line ratios. It provides insights into the

dominant mechanisms that power the emission lines observed in the spectra of galaxies. We use the line flux ratio of  $[\text{O III}]/\text{H}\beta$  vs.  $[\text{N II}]/\text{H}\alpha$ . The diagram is divided into the three regions containing purely star-forming or ‘HII region’ galaxies, composite galaxies, and galaxies with AGN based on prescription given by Kewley et al. (2001) and Kauffmann et al. (2003a).

The emission line fluxes used in the diagram were corrected for internal extinction prior to use. The reddening  $E(B - V)$  value was determined using  $\text{H}\alpha$  and  $\text{H}\beta$  emission lines following the Balmer decrement method given by Osterbrock (1989). It can be seen in the bottom left panel of Figure 3 that filaments contain a mix of populations in terms of nuclear activity. All purely star-forming galaxies in the FOVs were detected in FUV observation. We also detect a few galaxies with Active Galactic Nuclei (AGN) in our UV survey. The AGN-host filament galaxies are star-marked in Table 2.

#### 4.3. Morphological classification using non-parametric methods

We employ a non-parametric approach to determine the morphological classification of filament galaxies studied in this work. This method requires us to compute the Gini and M20 coefficients. The Gini coefficient ( $G$ ) is a statistical parameter based on the Lorentz curve (Lotz et al. 2004). The parameter is computed with the following equation:

$$G = \frac{1}{\bar{X}n(n-1)} \sum_i^n (2i - n - 1)X_i \quad (1)$$

here,  $X_i$  represents all pixel value,  $\bar{X}$  is the average of all  $X_i$ ,  $n$  is total number of pixels. All pixel values are arranged in an increasing order before calculating the  $G$ . For a homogeneous system,  $G$  converges to 0, whereas  $G = 1$  when the entire light of a galaxy is concentrated in a pixel (Glasser 1962).

The parameter  $M20$  corresponds to the second-order moment of light for the brightest region in the galaxy (Lotz et al. 2004). The parameter is calculated by summing over the brightest pixel values ( $f_i$ ) until the sum corresponds to 20% of the total galaxy flux. This value is normalized by  $M_{\text{tot}}$  corresponding to the second-order moment of the total light in a galaxy. These quantities are defined as:

$$M_{\text{tot}} = \sum_i^n M_i = \sum f_i [(x_i - x_c)^2 + (y_i - y_c)^2] \quad (2)$$

$$M_{20} = \log \left( \frac{\sum_i^n M_i}{M_{\text{tot}}} \right), \text{ where } \sum_i f_i < 0.2 f_{\text{tot}} \quad (3)$$

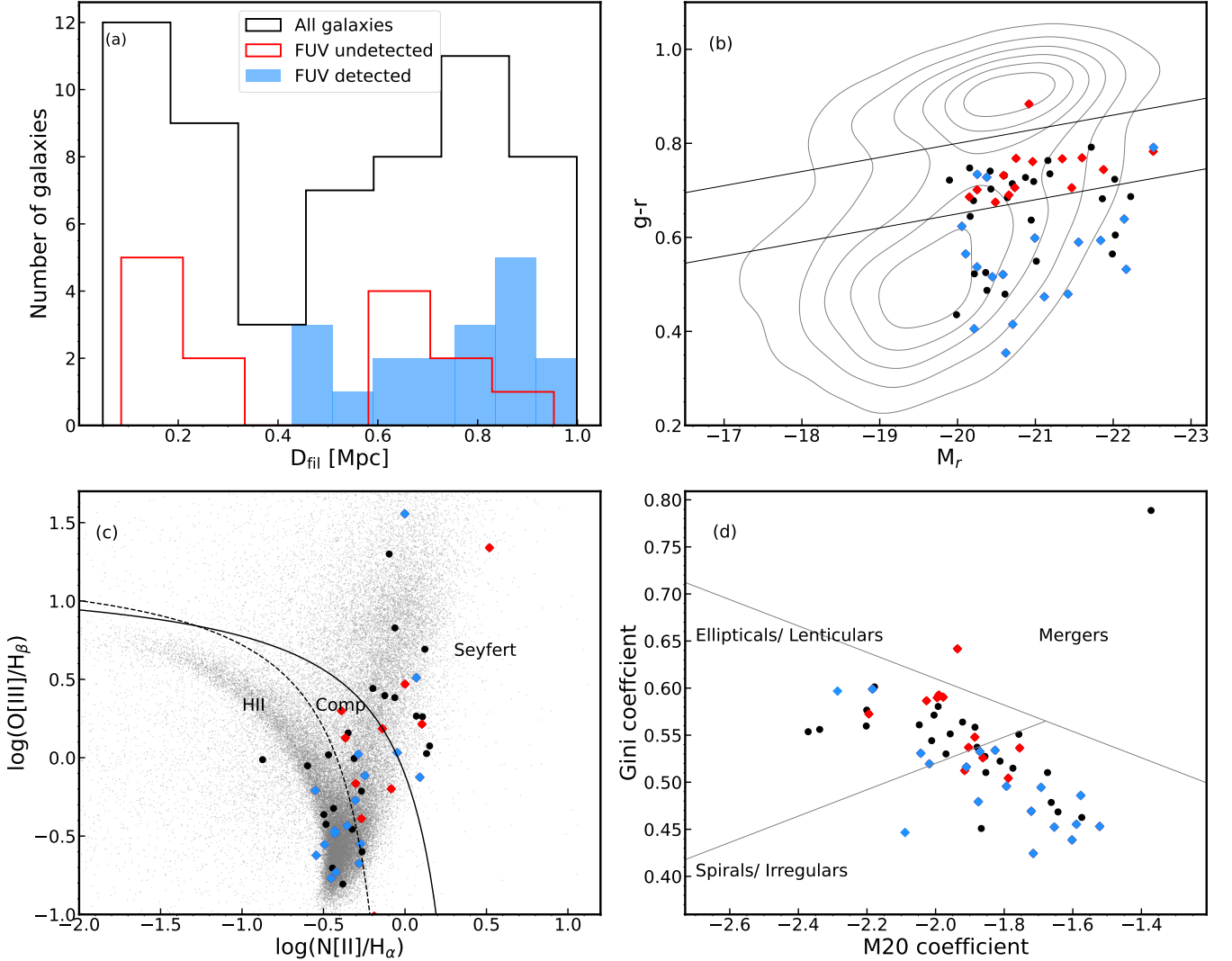


**Figure 3.** (a) Distribution of distance from the filament spine ( $D_{\text{fil}}$ ) for all filament galaxies (black) with  $D_{\text{fil}} \leq 1$  Mpc, galaxies detected (blue) and undetected (red) in our UVIT FUV survey. (b)  $g-r$  vs.  $M_r$  color-magnitude diagram for filament galaxies. The contour is composed of sample of local galaxies observed in *SDSS* DR 16. (c) BPT diagram used to separate HII region galaxies from composite and seyfert galaxies. The solid and dashed polynomial are described in Kewley et al. (2001) and Kauffmann et al. (2003a), respectively. Each grey dot represents a galaxy present in Kauffmann et al. (2003b) spectroscopic catalog. (d) Gini coefficient vs.  $M20$  coefficient for all filament galaxies. The markers have the same meaning as (a).

here,  $x_c$ ,  $y_c$  corresponds to galaxy central coordinates.

We use *statmorph*, a python-based code provided by Rodriguez-Gomez et al. (2019) to calculate the above-defined statistical parameters for *SDSS*  $r$ -band images of all filament galaxies. The code creates internal segmentation maps for the galaxies by using a threshold value for source detection and convolution filter size, both given by the user. The maps are used for calculating  $G$  and  $M20$ . The galaxies whose fitting was suspected were not included in the analysis.

The bottom right panel of Figure 3 shows the distribution for all filament galaxies. We refer to Lotz et al. (2008) for demarcating the galaxy population into spi-

rals/ irregular, elliptical/ lenticular, and merger candidates on  $G$  vs.  $M20$  plane. The filament galaxies from our study are equally distributed in the late- and early-type galaxy regions. Only two clear cases of galaxy merger have been identified in the sample. These galaxies appear to have elliptical morphology. We primarily detect disky-spiral galaxies in our UVIT FUV survey. Filaments contain mixed galaxy populations compared to void galaxies, which are primarily blue and disky in morphology (Kreckel et al. 2012; Pandey et al. 2021).

## 5. FUV EMISSION IN FILAMENT GALAXIES

The FUV SFRs would serve as an excellent tool to identify the most recently star-forming galaxy in our

**Table 2.** Detailed information on all 18 galaxies detected in UVIT FUV survey.

ID	RA	Dec	z	D <sub>fil</sub>	FUV	FUV SFR	M <sub>*</sub>	Fil ID
(1)	[deg]	[deg]	(4)	[Mpc]	[mag]	[M <sub>⊙</sub> yr <sup>-1</sup> ]	[M <sub>⊙</sub> ]	(9)
1	215.894	46.176	0.072	0.90	19.784 ± 0.042	2.372 ± 0.100	10.14	9987
2	217.090	45.966	0.074	0.61	21.247 ± 0.088	0.855 ± 0.076	10.65	4188
3	216.988	46.202	0.073	0.53	19.660 ± 0.042	1.993 ± 0.085	10.110	1029
4	215.788	46.289	0.073	0.45	20.347 ± 0.056	1.919 ± 0.108	10.22	9987
5*	215.819	46.146	0.073	0.98	20.594 ± 0.074	8.309 ± 0.612	11.20	9987
6	217.159	46.123	0.074	0.46	21.710 ± 0.102	0.880 ± 0.089	10.30	1029
7	215.817	46.028	0.073	0.81	21.440 ± 0.091	0.652 ± 0.059	10.02	9374
8	215.670	46.075	0.073	0.78	20.911 ± 0.080	1.017 ± 0.082	10.26	9374
9	215.772	46.149	0.074	1.00	19.649 ± 0.043	8.119 ± 0.350	10.78	9987
10	215.903	46.111	0.072	0.85	19.580 ± 0.041	4.851 ± 0.199	11.00	9374
11	217.302	46.240	0.075	0.85	20.410 ± 0.078	0.832 ± 0.065	9.91	1029
12	215.947	46.058	0.072	0.88	21.175 ± 0.082	1.006 ± 0.083	10.11	9374
13	217.152	46.316	0.075	0.88	19.206 ± 0.037	3.415 ± 0.126	10.58	1029
14	217.145	46.307	0.074	0.78	23.200 ± 0.256	0.084 ± 0.022	10.28	1029
15	215.838	46.247	0.072	0.74	19.629 ± 0.046	2.975 ± 0.138	10.50	9987
16*	215.941	45.931	0.072	0.74	18.890 ± 0.033	2.977 ± 0.100	11.34	9374
17*	217.108	45.969	0.074	0.43	22.755 ± 0.175	0.0023 ± 0.0004	11.41	1029
18*	215.848	45.905	0.072	0.67	24.893 ± 0.466	0.008 ± 0.004	10.30	9374

Col. (1) Identity number of each galaxy; (2), (3), and (4) represent the coordinates and redshift; (5) distance of each galaxy from the nearest filament spine; (6) FUV magnitudes (uncorrected for internal and galactic extinction); (7) intrinsic FUV SFRs; (8) stellar mass; (9) Serial number of the parent filament taken from [Tempel et al. \(2014\)](#). The star-marked galaxies in the table host an AGN.

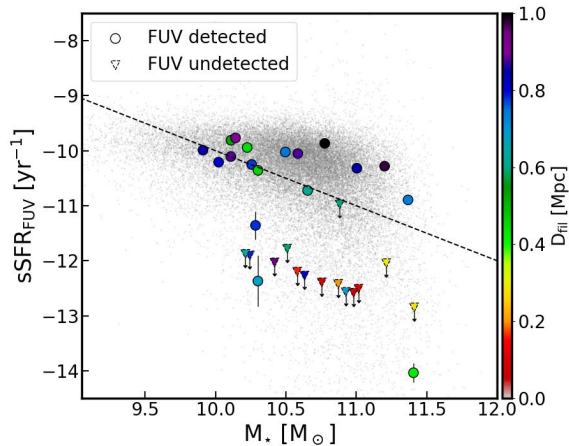


**Figure 4.** FUV sSFR vs. M<sub>\*</sub> for UVIT detected and undetected filament galaxies. The downward triangular markers indicate the upper limit of FUV sSFR. The color bar represents the D<sub>fil</sub> for each galaxy. Background galaxies shown with grey markers are taken from [Salim et al. \(2016\)](#).

sample. As highlighted in the previous section, apart from UVIT-identified galaxies, we find a set of filament galaxies that do not emit in FUV above a threshold

of  $1.5\sigma$ . These galaxies are termed as FUV undetected. We perform fixed aperture photometry with an aperture radius of  $\approx 1.5''$  on the FUV images at the centroid positions of the undetected galaxies. The magnitudes, thus obtained, were aperture corrected up to the saturation radius of a point source. The average aperture corrected magnitudes were approximately 1 - 1.5 mag higher than the FUV  $3\sigma$  limiting magnitude. These magnitudes are used in the subsequent analysis in this work.

We calculated internal extinction corrected FUV SFRs for all (UVIT detected and undetected) filament galaxies using following relation taken from [Kennicutt \(1998\)](#):

$$\text{SFR} = 1.4 \times L_{\text{FUV}} (\text{erg s}^{-1} \text{Hz}^{-1}) \quad (4)$$

Where  $L_{\text{FUV}}$  is the intrinsic FUV luminosity. We determine the value of internal extinction by the method discussed earlier in section 4.2. The ratio between stellar-to-gas attenuation is assumed to be 0.44. The median FUV SFRs of UVIT detected filament galaxies is  $\approx 1.0 M_{\odot} \text{ yr}^{-1}$ , similar to the Milky Way galaxy. The stellar mass of filament galaxies were procured from GALEX-SDSS-WISE Legacy Catalog (GSWLC, [Salim et al. 2016](#)). Table 2 contains the FUV magnitudes, SFRs, stellar mass, and D<sub>fil</sub> for all filament galaxies de-

tected in UVIT. Figure 4 shows FUV specific star formation rates ( $sSFR = SFR/M_*$ ) vs.  $M_*$  distribution for all filament galaxies targeted in our UVIT survey. We use aperture-corrected FUV magnitudes for calculating FUV SFRs in the case of UVIT undetected galaxies. The color bar indicates the  $D_{\text{fil}}$  for each galaxy.

As seen in the figure, we find two distinct populations of galaxies in the filaments - star-forming and quiescent. A majority of the UVIT undetected galaxies lie closer to the filament spine. The non-detection of galaxies near the spine could be associated with the extra-galactic gas supply cutoff deep inside filaments suggested by Kuutma et al. (2017), which may lead to a dearth of recent star formation in the region. We find a weak positive trend between FUV  $sSFR$  and  $D_{\text{fil}}$ . A similar trend of decreasing optical color index is reported in the literature (Kuutma et al. 2017; Singh et al. 2020). The relation is extensively discussed in the following section.

The massive filament galaxies ( $M_* \approx 10^{11} M_\odot$ ) detected in our FUV survey are mostly star-forming. Some of these galaxies also host an AGN. However, it is well-established that several stellar mass quenching processes, viz. gravitation quenching (Genzel et al. 2014), AGN feedback (Croton et al. 2006), active in massive galaxies lead to the cessation of the ongoing star formation. Intriguingly, a few studies on filaments establish that the inter-filamentary gas can replenish the HI content of filament galaxies (Kereš et al. 2005). Kleiner et al. (2017) reported the evidence of cold-mode gas accretion in several galaxies. This effect is more prominently observed in high-mass galaxies due to their deep gravitational potential well. As detected in our study, the accumulated cold gas can further ignite the star formation activities in the massive filament galaxies. However, the likelihood of gas accretion in the sampled filament galaxies needs further investigation.

### 5.1. Filament vs. clusters galaxies

One of the key objectives of this work is to investigate whether the star-forming properties of filament galaxies are different from those existing in other large-scale environments. Most of the galaxies detected in our FUV survey lie on the massive side of the stellar mass range. We do not include void galaxies in this analysis as voids are mostly dominated with low-stellar mass galaxies (Kreckel et al. 2012; Pandey et al. 2021). Galaxy clusters are another LSS known to host the most massive galaxies in the Universe. We compare two aspects of the FUV emission from cluster and filament galaxies. Firstly, we are interested in studying the gradient in FUV  $sSFR$ s of galaxies inside filaments and clusters as a function of their distances from the centers of the re-

spective structures. Moreover, we are motivated to compare the FUV emission in massive filament and cluster galaxies.

We use the RedMaPPer catalog (Rykoff et al. 2016) for identifying cluster galaxies in the nearby Universe ( $z < 0.1$ ). We select galaxies with cluster membership probability greater than 50%. The FUV magnitudes of cluster members were obtained from the *GALEX* AIS catalog. The galaxies with FUV magnitude error less than 0.3 mag are included in the sample. Using the FUV magnitudes, we calculate internal dust extinction FUV SFR using Equation 4. The value of internal reddening in the galaxies is deduced using the Balmer decrement ratio method (see Section 4.2). The stellar masses corresponding to the galaxies were taken from GSWLC. Forth applying all the cuts, we obtain a small sample of 33 cluster galaxies between a mass range of  $10^{10.4} M_\odot$  to  $10^{11.8} M_\odot$ .

Figure 5 depicts the dependence of FUV  $sSFR$  on the distance of filament spine and cluster center for filament and cluster galaxies, respectively. We include FUV undetected galaxies in the analysis for a coherent interpretation. It can be clearly seen that the recent star formation for filament galaxies decreases on approaching the filament spine. On the other hand, cluster galaxies show little-to-no dependence between FUV  $sSFR$ s and distance from the cluster center. Previously done studies pointed out that for nearby galaxies ( $z \sim 0$ ), the SFR and  $sSFR$  do not show any significant variation with clustercentric distance (Laganá & Ulmer 2017). Even after including FUV undetected filament galaxies in the study, the correlation between  $sSFR$  and  $D_{\text{fil}}$  remains unaltered. The results highlight the difference in evolution galaxies depending on the large-scale environment.

Figure 5 qualitatively shows that the average FUV  $sSFR$  of filament galaxies detected in FUV observation is greater than the cluster galaxies. We perform the Kolmogorov-Smirnov (KS) test and the Anderson-Darling (AD) test on the distribution of FUV  $sSFR$  for cluster and filament galaxies in a fixed stellar mass bin. We only selected galaxies having stellar mass greater than  $10^{10.5} M_\odot$ . The p-values corresponding to both tests were much less than 0.05, whereas KS-statistic (= 0.73) and AD-statistic (= 7.2) were high on comparing the FUV  $sSFR$  of UVIT detected filament and cluster galaxies. We combine the aperture-corrected FUV  $sSFR$  of undetected filament galaxies with the detected galaxies and perform the same statistical tests. The p-value increases to 0.02, less than the significance level of 0.05. Hence, we conclude that the FUV  $sSFR$  of massive filament and cluster galaxies belong to different parent populations. The statistical tests imply that the star

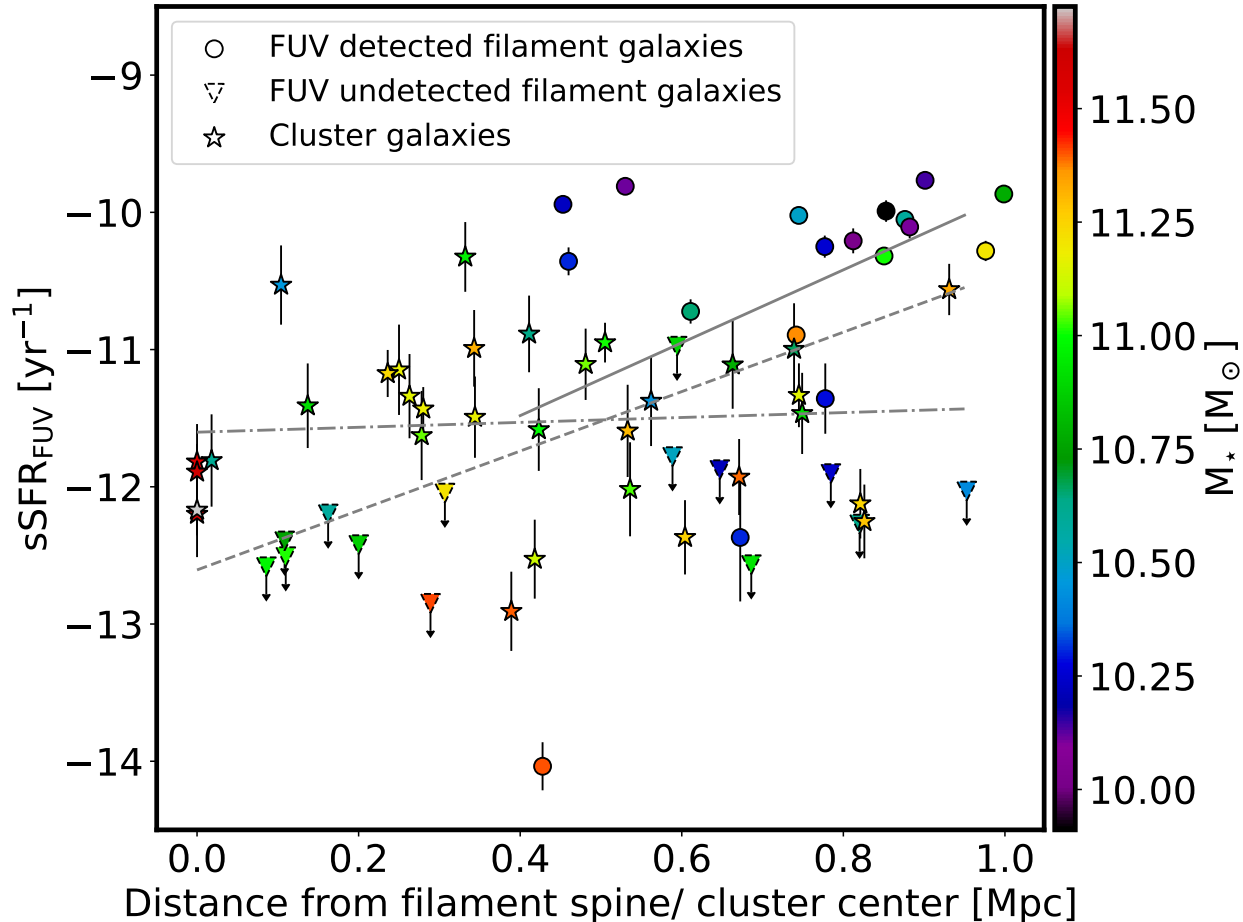


**Figure 5.** Variation of FUV sSFR in filament/ cluster galaxies as a function of the distance of galaxies from the filament spine/ cluster center. The FUV detected, and undetected filament galaxies are shown with circle and downward triangle symbols. The downward arrow used for FUV undetected filament galaxies shows the upper limit of FUV sSFR calculated using aperture-corrected FUV magnitude. Star markers represent the cluster galaxies. The best linear fit over the cluster and filament galaxy (detected/ detected and undetected) distributions are represented with grey dash-dotted and solid/ dashed lines, respectively. The color bar represents the stellar mass of galaxies.

formation process is more rapid in filaments than clusters. The observed results could arise from a slower gas depletion time scale in the former environment than the latter one, as pointed out by [Castignani et al. \(2022\)](#). Alternatively, the cold mode gas accretion from inter-filamentary channels or gas-rich mergers could rejuvenate the star formation in massive galaxies.

### 5.2. FUV morphology of filament galaxies

The FUV morphology of galaxies is an efficient probe to identify the recently star-forming regions in them. We utilize our well-resolved UVIT observation to investigate the FUV morphology of filament galaxies and compare

them with their optical counterparts. Figure 6 illustrates FUV images of all UVIT-detected filament galaxies. The blue contours on the figure show the *SDSS*-r band profile of galaxies. The three contour levels in blue represent  $10\sigma$ ,  $5\sigma$ , and  $1.5\sigma$  level, where  $\sigma$  represents the mean standard deviation in the *SDSS* r-band observation. The surface brightness of the outermost contour is  $24.14 \text{ mag arcsec}^{-2}$ . The galaxies are serially assigned a number (*ID*) according to Table 2.

We show FUV and optical centroids of the galaxies using cyan and red crosses, respectively. The young stellar population inside galaxies represented by FUV emission mostly aligns with the main stellar population

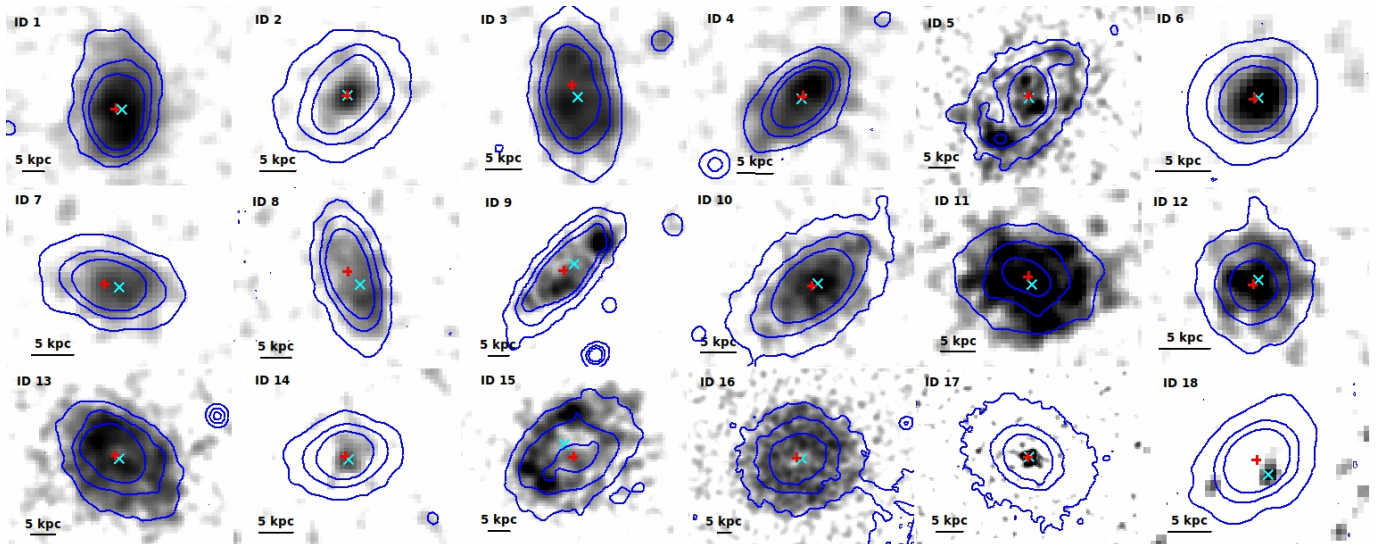


**Figure 6.** Grey-scale FUV image stamps of all 18 galaxies detected in the FUV survey are shown. The optical morphology in *SDSS* r-band is superimposed on the image stamps. The three levels of the blue contours represent  $10\sigma$ ,  $5\sigma$ , and  $1.5\sigma$  threshold level above the background noise. The surface brightness of the outermost contour is  $24.14 \text{ mag arcsec}^{-2}$ . The identity number, stellar mass, and distance of galaxies from the nearest filament are mentioned on each image from top to bottom. We mark the centroids of FUV and r-band observation with cyan and red crosses, respectively.

traced by optical emission. On the contrary, a similar analysis done for cluster galaxies by Mahajan et al. (2022) highlights that the FUV morphology for a sample of cluster galaxies was skewed relative to their optical emission primarily due to ram-pressure stripping (Gunn & Gott 1972) rampantly observed in the cluster environment. The result establishes that filament galaxies may not witness extreme environment disturbances, which are prevalent in clusters. However, the FUV emission appears clumpy in the filament galaxies and shows considerable size variation. For a few galaxies, the emission is asymmetric within the galaxy, e.g., *ID 9*, *ID 15*. Moreover, we observe FUV emission in some galaxies beyond the outermost optical contour, e.g., *ID 1*, *ID 5*, *ID 11*, *ID 15*. These observations hint at the possibility of recent gas accretion episodes. A thorough comparison between deep optical and UV observation of the filament galaxies is required for confirming the existence of extended-UV disks (Thilker et al. 2007).

As discussed in the previous section, massive galaxies in filament exhibit a faster rate of recent star formation than those in the clusters. The FUV disk sizes of most of the massive filament galaxies ( $M_{\star} > 10^{10.5} M_{\odot}$ ) in the sample are slightly extended or comparable to their optical emission. These galaxies are mostly detected in the outer edge of filaments ( $D_{\text{fil}} \sim 0.9 \text{ Mpc}$ ). Previous studies establish that high stellar mass galaxies primarily reside closer to the filament spine (Chen et al. 2017). In our survey, massive galaxies near the filament axis were undetected or detected with weak UV emis-

sion (see *ID 17* in Figure 6; also see upper left panel of Figure 3). Some moderate stellar mass galaxies ( $\lesssim 10^{10.5} M_{\odot}$ ) also show extended UV emission in our sample (e.g., *ID 11*). Previous discussion in this work hints towards a gradient in the level of recent star formation as we progress from the filament axis to its outer edges. An earlier study analyzing the HI gas content of galaxies in the filament environment reported that at fixed stellar mass and color, the galaxies closer to the filament spine are increasingly HI deficient (Odekon et al. 2018). This finding corroborates our result wherein the galaxies closer to the spine do not show a signature of recent star formation.

## 6. IMPACT ON THE MASS ASSEMBLY

The results presented in the previous sections establishes that the filaments provide an in-homogeneous environment for galaxies to evolve. We detect a negative gradient in FUV sSFRs on approaching the filament spine. Moreover, we find hints of gas accretion on the filament galaxies by comparing their UV and optical morphology. The observations suggest existence of physical mechanisms, such as galaxy interaction, gas starvation, inside filaments. The study of the stellar mass assembly of filament galaxies would highlight the mechanisms dominantly influencing their evolution. Multiple physical in-situ and externally driven processes may lead to stellar mass accumulation in galaxies over the cosmic time. The in-situ process includes star formation, gas recycling, and gas accretion from the inter-galactic medium (Fall & Efstathiou 1980; Carroll & Ostlie 2017)

whereas merger-interaction, accretion of satellite galaxies, gas stripping (Toomre et al. 1977) are a few externally driven processes that steer stellar mass growth. There are two prominent mass assembly mechanisms are thought to be in action in galaxies, i.e., ‘inside-out’ and ‘outside-in’ modes in the literature (Sánchez-Blázquez et al. 2007; Pérez et al. 2013; Pan et al. 2015). In the case of inside-out mass assembly, the central regions of a galaxy form stars earlier and more rapidly than the outer regions. Outside-in growth, on the other hand, describes a pattern where star formation starts in the outer regions of a galaxy and then progresses inward toward the central region. The secularly evolving galaxies mainly grow via an inside-out mechanism whereas galaxies influenced due to environment show outside-in stellar mass build-up.

Broadband colors of galaxies are often used to determine stellar population age of galaxies in case of unavailability of spectral information. In this section, we use UV-optical ( $FUV - r$ ) color index to indicate stellar population age. The ( $FUV - r$ ) color is used actively to segregate star-forming and passive galaxies (Hammer et al. 2012). Both *SDSS* and UVIT have similar resolution and pixel scale ( $\sim 0.''4$ ). We perform photometry on a central aperture of  $r = 1.5''$  as it is roughly comparable to the point-source function full-width half maxima (PSF FWHM) of the two surveys. The radius is equivalent to  $\approx 2.25$  kpc at  $z$  between 0.07 and 0.08. We consider the Petrosian magnitude of the sources as a measure of their total magnitude. The color gradient,  $\Delta(FUV - r)$ , is computed using the following equation:

$$\Delta(FUV - r) = (FUV - r)_{r=1.5''} - (FUV - r)_{\text{total}} \quad (5)$$

We divide our galaxy sample into three categories based on the value of  $\Delta(FUV - r)$ . The color gradient is positive ( $> 2\sigma$ ) for red-cored galaxies whereas  $\Delta(FUV - r) < 2\sigma$  for blue-cored galaxies. The galaxies with  $|\Delta(FUV - r)| < 2\sigma$  are considered flat-cored. The average error ( $\sigma$ ) associated with ( $FUV - r$ ) color is 0.12 mag.

We calculate the ratio of FUV SFR within a circular aperture of radius  $\sim 1.''5$  to total FUV SFR. The left panel of Figure 7 shows the central-to-total SFR ratio vs.  $\Delta(FUV - r)$  distribution for filament galaxies. Here, galaxies belonging to the blue cloud in the upper right panel of Figure 3 are termed star-forming, whereas the remaining sample detected in UVIT is grouped as quenched. The quenched galaxies in the sample have the most negative color gradients, similar to blue-cored galaxies. The star formation in these galaxies is restricted to the inner region. On the other hand, the

red-cored filament galaxies have comparable FUV SFR throughout their extent.

The variation of  $\Delta(FUV - r)$  and  $D_{\text{fil}}$  is shown in the right panel of Figure 7. The sample has a nearly equal number of red- and blue-cored filament galaxies. Galaxies with  $M_{\star} < 10^{10.5} M_{\odot}$  mostly have flat color gradients with few exceptions showing a blue-core. Nearly all galaxies closer to the filament spine, i.e.,  $D_{\text{fil}} \lesssim 0.7$  Mpc, are blue-cored regardless of their stellar masses. The result implies that these galaxies are likelier to witness galaxy nurture activities. The galaxies situated radially outwards in the filament are red-cored or, in other words, follow ‘inside-out’ mass assembly. We compare the strength of the monotonic relation between  $\Delta(FUV - r)$  and  $D_{\text{fil}}$  against  $\Delta(FUV - r)$  and  $M_{\star}$  by computing their Spearman correlation coefficient ( $\rho_s$ ) for both pairs. The quantity  $D_{\text{fil}}$  proxy for the environment ( $\rho_s = 0.377$  with a p-value of 0.123) has a stronger positive correlation compared to the stellar mass ( $\rho_s = 0.226$  with a p-value of 0.367). We conclude that the environment has a more substantial influence on the mass assembly of filament galaxies. However, it is essential to note that both correlations are positive and relatively weak.

## 7. DISCUSSION AND CONCLUSIONS

This study aims at understanding the star formation properties of galaxies inside filaments. We conduct a deep FUV survey to identify galaxies undergoing recent star formation and to subsequently investigate their FUV sSFRs, FUV morphology, and mass-assembly mechanism. The results are compared with cluster galaxies in a fixed stellar mass range. Although the filament comprises both early- and late-type galaxies, we mostly detect star-forming and disk galaxies in our FUV survey. Our UV survey does not detect galaxies closer than 0.4 Mpc from the spine. Previous studies have pointed out that the fraction of elliptical galaxies increases as the distance towards the filament axis decreases (Kuutma et al. 2017). The massive or red galaxies are more likely to exist near the spine of the filament (Chen et al. 2017). The non-detection of such galaxies in our deep UV survey confirms their dearth of star formation deep inside filaments. The mixed galaxy population type detected in filament could result from the pre-processing of galaxies inside filaments (Castignani et al. 2022).

Moreover, we find a trend between the recent star formation timescale in galaxies with  $D_{\text{fil}}$ . The galaxies at the filament outskirts are more star-forming than those in the inner region. The result corroborates the finding of Kuutma et al. (2017), where the spiral galaxy fraction

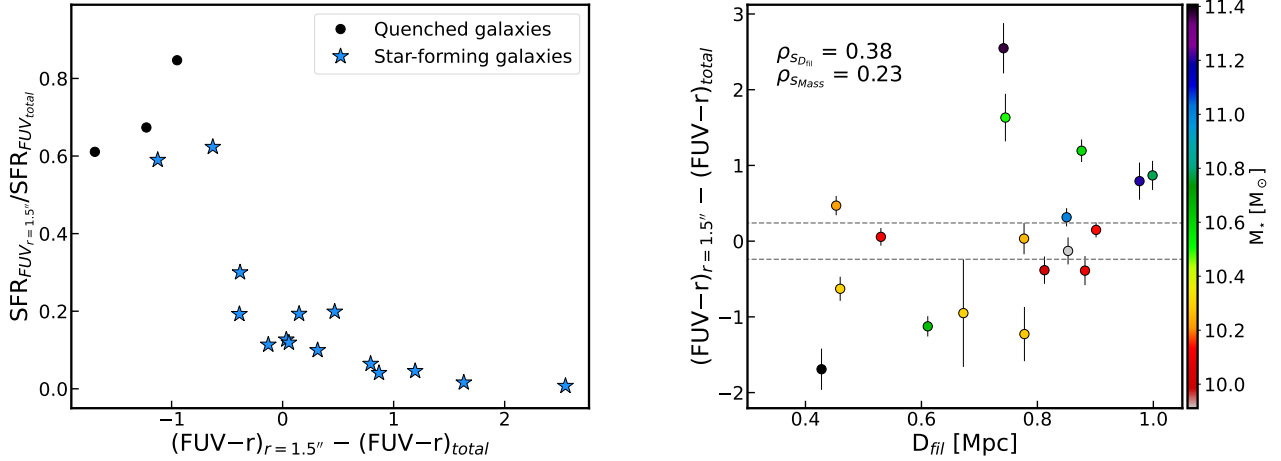


**Figure 7.** Left panel: Ratio of FUV SFR (aperture size ( $r$ ) = 1.5'' and Petrosian aperture) vs.  $\Delta(FUV - r)$ . Right panel: Distribution of  $\Delta(FUV - r)$  and  $D_{\text{fil}}$ . The color bar shown in the image represents stellar mass of individual filament galaxies. The horizontal lines enclose the region representing flat-color gradient galaxies.

increases with increasing distance from the spine of the filament. On comparing the observed trend with the cluster environment, the sSFR of filament galaxies increases as a function of distance to the filament axis. In contrast, cluster galaxies show no such effects. A previous study on cluster galaxies shows very slight variation wherein the sSFR of galaxies increases slightly when approaching cluster center (Laganá & Ulmer 2017). According to a comparative study done by Mahajan et al. (2018) on filament, void, and cluster galaxies observes a similar result by analyzing their  $H_{\alpha}$  equivalent width and colors. Ricciardelli et al. (2014) found a decrease in the SFR as distance from the void center increases up to a certain mean distance while no effect could be established for sSFRs of galaxies. The discussion above illustrates the difference in the evolution of galaxies in various LSSs. A comprehensive study combining more UV observations of LSSs would be aimed.

In this study, we observe that galaxies with  $M_*$  than  $10^{11} M_{\odot}$  placed in the outer region of filaments have equivalent or slightly extended FUV disk size compared to their optical counterpart. The result may be an outcome of cold-mode gas accretion on the galaxies through filaments. However, some of these galaxies host AGN or are surrounded by close neighboring galaxies, which may have led to the observed result. Therefore, our study could neither confirm nor deny the cold mode accretion process reported by Kleiner et al. (2017). Agreeably, we detected a limited number of filament galaxies detected in our UVIT survey. Hence, we aim to perform a similar study with an increased sample to enhance our understanding of filament galaxies. Deep multi-band ob-

servations could be utilized to undermine the prevalence cold-mode gas accretion in filaments.

We study the mass assembly of filament galaxies based on  $(FUV - r)$  color gradient. The galaxies closer to the filament spine mainly evolve via outside-in growth mass assembly. In other words, galaxies host blue cores closer to the filament axis. Similar results were reported by Lee et al. (2021), where the distribution of  $H_{\alpha}$  equivalent width as a function of vertical distance from the filament axis was studied. The author showed that the high stellar mass galaxies closer to the filament spine are actively star-forming in their central region. A considerable cause of the central star formation could be the increased likelihood of merger interactions.

Our work establishes that filament could serve as a hotbed for several activities impacting the growth of galaxies residing inside filaments., e.g., galaxy interactions, gas starvation, and gas accretion. These processes attribute to a range of galaxy properties in color, SFR, and morphology. The results from our study are summarized below:

- i) We detect galaxies with  $D_{\text{fil}} > 0.4$  Mpc in our deep UV survey.
- ii) The study establishes that the filament environment substantially affects the evolution of galaxies inside them. We find early- and late-type galaxies residing inside the filament. Most of the galaxies detected by in our FUV survey are star-forming and late-type.
- iii) There is a positive gradient in FUV sSFR as the distance from the filament axis increases.
- iv) We find that massive galaxies in the filament are undergoing recent star formation on a rapid timescale

compared to galaxies in clusters.

v) The UV morphology for a few galaxies residing in the outer edge of filaments is extended more than their optical profile.

vi) ‘Outside-in’ mass-assembly mode is more prevalent in the inner region of the filaments, i.e., galaxies inside filaments are centrally star-forming. The result could be due to an increased rate of galaxy merger interaction in the inner region.

1 This publication uses the data from the AstroSat mis-  
2 sion of the Indian Space Research Organisation (ISRO)  
3 archived at the Indian Space Science Data Centre  
4 (ISSDC). DP and ACP would like to acknowledge In-  
5 ter University Centre for Astronomy and Astrophysics  
6 (IUCAA), Pune, India for providing facilities to carry  
7 out this work.

*Facilities:* *AstroSat/UVIT, GALEX, SDSS*

*Software:* CCDLAB (Postma & Leahy 2021),  
Source Extractor (Bertin & Arnouts 1996), StatMorph  
(Rodriguez-Gomez et al. 2019)

## REFERENCES

- Ahumada, R., Allende Prieto, C., Almeida, A., et al. 2020, *ApJS*, 249, 3, doi: [10.3847/1538-4365/ab929e](https://doi.org/10.3847/1538-4365/ab929e)
- Alpaslan, M., Robotham, A. S. G., Driver, S., et al. 2014, *MNRAS*, 438, 177, doi: [10.1093/mnras/stt2136](https://doi.org/10.1093/mnras/stt2136)
- Alpaslan, M., Grootes, M., Marcum, P. M., et al. 2016, *MNRAS*, 457, 2287, doi: [10.1093/mnras/stw134](https://doi.org/10.1093/mnras/stw134)
- Aragon Calvo, M. A., Neyrinck, M. C., & Silk, J. 2019, *The Open Journal of Astrophysics*, 2, 7, doi: [10.21105/astro.1697.07881](https://doi.org/10.21105/astro.1697.07881)
- Baldwin, J. A., Phillips, M. M., & Terlevich, R. 1981, *PASP*, 93, 5, doi: [10.1086/130766](https://doi.org/10.1086/130766)
- Bertin, E., & Arnouts, S. 1996, *A&AS*, 117, 393, doi: [10.1051/aas:1996164](https://doi.org/10.1051/aas:1996164)
- Blanton, M. R., Dalcanton, J., Eisenstein, D., et al. 2001, *AJ*, 121, 2358, doi: [10.1086/320405](https://doi.org/10.1086/320405)
- Blanton, M. R., Schlegel, D. J., Strauss, M. A., et al. 2005, *AJ*, 129, 2562, doi: [10.1086/429803](https://doi.org/10.1086/429803)
- Bonjean, V., Aghanim, N., Douspis, M., Malavasi, N., & Tanimura, H. 2020, *A&A*, 638, A75, doi: [10.1051/0004-6361/201937313](https://doi.org/10.1051/0004-6361/201937313)
- Carroll, B. W., & Ostlie, D. A. 2017, *An Introduction to Modern Astrophysics*, 2nd edn. (Cambridge University Press), doi: [10.1017/9781108380980](https://doi.org/10.1017/9781108380980)
- Carrón Duque, J., Migliaccio, M., Marinucci, D., & Vittorio, N. 2022, *A&A*, 659, A166, doi: [10.1051/0004-6361/202141538](https://doi.org/10.1051/0004-6361/202141538)
- Castignani, G., Combes, F., Jablonka, P., et al. 2022, *A&A*, 657, A9, doi: [10.1051/0004-6361/202040141](https://doi.org/10.1051/0004-6361/202040141)
- Cautun, M., van de Weygaert, R., & Jones, B. J. T. 2013, *MNRAS*, 429, 1286, doi: [10.1093/mnras/sts416](https://doi.org/10.1093/mnras/sts416)
- Cautun, M., van de Weygaert, R., Jones, B. J. T., & Frenk, C. S. 2014, *MNRAS*, 441, 2923, doi: [10.1093/mnras/stu768](https://doi.org/10.1093/mnras/stu768)
- Chen, Y.-C., Ho, S., Mandelbaum, R., et al. 2017, *MNRAS*, 466, 1880, doi: [10.1093/mnras/stw3127](https://doi.org/10.1093/mnras/stw3127)
- Colberg, J. M., Krughoff, K. S., & Connolly, A. J. 2005, *MNRAS*, 359, 272, doi: [10.1111/j.1365-2966.2005.08897.x](https://doi.org/10.1111/j.1365-2966.2005.08897.x)
- Croton, D. J., Springel, V., White, S. D. M., et al. 2006, *MNRAS*, 365, 11, doi: [10.1111/j.1365-2966.2005.09675.x](https://doi.org/10.1111/j.1365-2966.2005.09675.x)
- Darvish, B., Sobral, D., Mobasher, B., et al. 2014, *ApJ*, 796, 51, doi: [10.1088/0004-637X/796/1/51](https://doi.org/10.1088/0004-637X/796/1/51)
- Durret, F., Lima Neto, G. B., Forman, W., & Churazov, E. 2003, *A&A*, 403, L29, doi: [10.1051/0004-6361:20030424](https://doi.org/10.1051/0004-6361:20030424)
- Fall, S. M., & Efstathiou, G. 1980, *MNRAS*, 193, 189, doi: [10.1093/mnras/193.2.189](https://doi.org/10.1093/mnras/193.2.189)
- Gaia Collaboration, Prusti, T., de Bruijne, J. H. J., et al. 2016, *A&A*, 595, A1, doi: [10.1051/0004-6361/201629272](https://doi.org/10.1051/0004-6361/201629272)
- Galárraga-Espinosa, D., Aghanim, N., Langer, M., & Tanimura, H. 2021, *A&A*, 649, A117, doi: [10.1051/0004-6361/202039781](https://doi.org/10.1051/0004-6361/202039781)
- Genzel, R., Schreiber, N. M. F., Lang, P., et al. 2014, *ApJ*, 785, 75, doi: [10.1088/0004-637X/785/1/75](https://doi.org/10.1088/0004-637X/785/1/75)
- Gil de Paz, A., Boissier, S., Madore, B. F., et al. 2007, *ApJS*, 173, 185, doi: [10.1086/516636](https://doi.org/10.1086/516636)
- Ginsburg, A., Sipőcz, B. M., Brasseur, C. E., et al. 2019, *AJ*, 157, 98, doi: [10.3847/1538-3881/aafc33](https://doi.org/10.3847/1538-3881/aafc33)
- Glasser, G. J. 1962, *Journal of the American Statistical Association*, 57, 648, doi: [10.1080/01621459.1962.10500553](https://doi.org/10.1080/01621459.1962.10500553)
- Gunn, J. E., & Gott, J. Richard, I. 1972, *ApJ*, 176, 1, doi: [10.1086/151605](https://doi.org/10.1086/151605)
- Hammer, D. M., Hornschemeier, A. E., Salim, S., et al. 2012, *ApJ*, 745, 177, doi: [10.1088/0004-637X/745/2/177](https://doi.org/10.1088/0004-637X/745/2/177)
- Kauffmann, G., Heckman, T. M., Tremonti, C., et al. 2003a, *MNRAS*, 346, 1055, doi: [10.1111/j.1365-2966.2003.07154.x](https://doi.org/10.1111/j.1365-2966.2003.07154.x)

- Kauffmann, G., Heckman, T. M., White, S. D. M., et al. 2003b, *MNRAS*, 341, 33, doi: [10.1046/j.1365-8711.2003.06291.x](https://doi.org/10.1046/j.1365-8711.2003.06291.x)
- Kennicutt, R. C. 1998, *Annual Review of Astronomy and Astrophysics*, 36, 189, doi: [10.1146/annurev.astro.36.1.189](https://doi.org/10.1146/annurev.astro.36.1.189)
- Kereš, D., Katz, N., Weinberg, D. H., & Davé, R. 2005, *MNRAS*, 363, 2, doi: [10.1111/j.1365-2966.2005.09451.x](https://doi.org/10.1111/j.1365-2966.2005.09451.x)
- Kewley, L. J., Dopita, M. A., Sutherland, R. S., Heisler, C. A., & Trevena, J. 2001, *ApJ*, 556, 121, doi: [10.1086/321545](https://doi.org/10.1086/321545)
- Kirshner, R. P., Oemler, A., J., Schechter, P. L., & Shectman, S. A. 1981, *ApJL*, 248, L57, doi: [10.1086/183623](https://doi.org/10.1086/183623)
- Kleiner, D., Pimbblet, K. A., Jones, D. H., Koribalski, B. S., & Serra, P. 2017, *MNRAS*, 466, 4692, doi: [10.1093/mnras/stw3328](https://doi.org/10.1093/mnras/stw3328)
- Kreckel, K., Platen, E., Aragón-Calvo, M. A., et al. 2012, *AJ*, 144, 16, doi: [10.1088/0004-6256/144/1/16](https://doi.org/10.1088/0004-6256/144/1/16)
- Kuutma, T., Tamm, A., & Tempel, E. 2017, *A&A*, 600, L6, doi: [10.1051/0004-6361/201730526](https://doi.org/10.1051/0004-6361/201730526)
- Laganá, T. F., & Ulmer, M. P. 2017, *MNRAS*, 475, 523, doi: [10.1093/mnras/stx3210](https://doi.org/10.1093/mnras/stx3210)
- Laigle, C., Pichon, C., Arnouts, S., et al. 2018, *MNRAS*, 474, 5437, doi: [10.1093/mnras/stx3055](https://doi.org/10.1093/mnras/stx3055)
- Lee, J., & Pen, U.-L. 2000, *ApJL*, 532, L5, doi: [10.1086/312556](https://doi.org/10.1086/312556)
- Lee, Y., Kim, S., Rey, S.-C., & Chung, J. 2021, *ApJ*, 906, 68, doi: [10.3847/1538-4357/abcaa0](https://doi.org/10.3847/1538-4357/abcaa0)
- Liao, S., & Gao, L. 2019, *MNRAS*, 485, 464, doi: [10.1093/mnras/stz441](https://doi.org/10.1093/mnras/stz441)
- Lin, L., Hsieh, B.-C., Pan, H.-A., et al. 2019, *ApJ*, 872, 50, doi: [10.3847/1538-4357/aafa84](https://doi.org/10.3847/1538-4357/aafa84)
- Lotz, J. M., Primack, J., & Madau, P. 2004, *AJ*, 128, 163, doi: [10.1086/421849](https://doi.org/10.1086/421849)
- Lotz, J. M., Davis, M., Faber, S. M., et al. 2008, *ApJ*, 672, 177, doi: [10.1086/523659](https://doi.org/10.1086/523659)
- Mahajan, S., Singh, A., & Shobhana, D. 2018, *MNRAS*, 478, 4336, doi: [10.1093/mnras/sty1370](https://doi.org/10.1093/mnras/sty1370)
- Mahajan, S., Singh, K. P., Postma, J. E., et al. 2022, *PASA*, 39, e048, doi: [10.1017/pasa.2022.45](https://doi.org/10.1017/pasa.2022.45)
- Morrissey, P., Conrow, T., Barlow, T. A., et al. 2007, *ApJS*, 173, 682, doi: [10.1086/520512](https://doi.org/10.1086/520512)
- Odekon, M. C., Hallenbeck, G., Haynes, M. P., et al. 2018, *ApJ*, 852, 142, doi: [10.3847/1538-4357/aaa1e8](https://doi.org/10.3847/1538-4357/aaa1e8)
- Osterbrock, D. E. 1989, *Astrophysics of gaseous nebulae and active galactic nuclei*
- Pan, Z., Li, J., Lin, W., et al. 2015, *ApJL*, 804, L42, doi: [10.1088/2041-8205/804/2/L42](https://doi.org/10.1088/2041-8205/804/2/L42)
- Pandey, D., Saha, K., & Pradhan, A. C. 2021, *ApJ*, 919, 101, doi: [10.3847/1538-4357/ac1078](https://doi.org/10.3847/1538-4357/ac1078)
- Pérez, E., Cid Fernandes, R., González Delgado, R. M., et al. 2013, *ApJL*, 764, L1, doi: [10.1088/2041-8205/764/1/L1](https://doi.org/10.1088/2041-8205/764/1/L1)
- Porter, S. C., & Raychaudhury, S. 2005, *MNRAS*, 364, 1387, doi: [10.1111/j.1365-2966.2005.09688.x](https://doi.org/10.1111/j.1365-2966.2005.09688.x)
- Postma, J. E., & Leahy, D. 2021, *Journal of Astrophysics and Astronomy*, 42, 30, doi: [10.1007/s12036-020-09689-w](https://doi.org/10.1007/s12036-020-09689-w)
- Poudel, A., Heinämäki, P., Tempel, E., et al. 2017, *A&A*, 597, A86, doi: [10.1051/0004-6361/201629639](https://doi.org/10.1051/0004-6361/201629639)
- Ricciardelli, E., Cava, A., Varela López, J., & Quilis, V. 2014, *MNRAS*, 445, doi: [10.1093/mnras/stu2061](https://doi.org/10.1093/mnras/stu2061)
- Rodríguez-Gomez, V., Snyder, G. F., Lotz, J. M., et al. 2019, *MNRAS*, 483, 4140, doi: [10.1093/mnras/sty3345](https://doi.org/10.1093/mnras/sty3345)
- Rykoff, E. S., Rozo, E., Hollowood, D., et al. 2016, *ApJS*, 224, 1, doi: [10.3847/0067-0049/224/1/1](https://doi.org/10.3847/0067-0049/224/1/1)
- Salim, S. 2014, *Serbian Astronomical Journal*, 189, 1, doi: [10.2298/SAJ1489001S](https://doi.org/10.2298/SAJ1489001S)
- Salim, S., Lee, J. C., Janowiecki, S., et al. 2016, *ApJS*, 227, 2, doi: [10.3847/0067-0049/227/1/2](https://doi.org/10.3847/0067-0049/227/1/2)
- Sánchez-Blázquez, P., Forbes, D. A., Strader, J., Brodie, J., & Proctor, R. 2007, *MNRAS*, 377, 759
- Schlegel, D. J., Finkbeiner, D. P., & Davis, M. 1998, *ApJ*, 500, 525, doi: [10.1086/305772](https://doi.org/10.1086/305772)
- Singh, A., Mahajan, S., & Bagla, J. S. 2020, *MNRAS*, 497, 2265, doi: [10.1093/mnras/staa1913](https://doi.org/10.1093/mnras/staa1913)
- Sousbie, T., Pichon, C., & Kawahara, H. 2011, *MNRAS*, 414, 384, doi: [10.1111/j.1365-2966.2011.18395.x](https://doi.org/10.1111/j.1365-2966.2011.18395.x)
- Tandon, S. N., Subramaniam, A., Girish, V., et al. 2017, *AJ*, 154, 128, doi: [10.3847/1538-3881/aa8451](https://doi.org/10.3847/1538-3881/aa8451)
- Tandon, S. N., Postma, J., Joseph, P., et al. 2020, *AJ*, 159, 158, doi: [10.3847/1538-3881/ab72a3](https://doi.org/10.3847/1538-3881/ab72a3)
- Tempel, E., Guo, Q., Kipper, R., & Libeskind, N. I. 2015, *MNRAS*, 450, 2727, doi: [10.1093/mnras/stv919](https://doi.org/10.1093/mnras/stv919)
- Tempel, E., & Libeskind, N. I. 2013, *ApJL*, 775, L42, doi: [10.1088/2041-8205/775/2/L42](https://doi.org/10.1088/2041-8205/775/2/L42)
- Tempel, E., Stoica, R. S., Martínez, V. J., et al. 2014, *MNRAS*, 438, 3465, doi: [10.1093/mnras/stt2454](https://doi.org/10.1093/mnras/stt2454)
- Tempel, E., & Tamm, A. 2015, *A&A*, 576, L5, doi: [10.1051/0004-6361/201525827](https://doi.org/10.1051/0004-6361/201525827)
- Thilker, D. A., Bianchi, L., Meurer, G., et al. 2007, *The Astrophysical Journal Supplement Series*, 173, 538, doi: [10.1086/523853](https://doi.org/10.1086/523853)
- Toomre, A., Tinsley, B., & Larson, R. 1977, *Evolution of Galaxies and Stellar Populations*, Yale Univ. Observatory New Haven, CT
- Vulcani, B., Poggianti, B. M., Moretti, A., et al. 2019, *MNRAS*, 487, 2278, doi: [10.1093/mnras/stz1399](https://doi.org/10.1093/mnras/stz1399)